Shear-Induced Crystallization Precursor Studies in Model Polyethylene Blends by in-Situ Rheo-SAXS and Rheo-WAXD

Ling Yang,[†] Rajesh H. Somani,[†] Igors Sics,[†] Benjamin S. Hsiao,*[,†] Rainer Kolb,[§] Hitesh Fruitwala,[§] and Christine Ong[‡]

Department of Chemistry, State University of New York at Stony Brook, Stony Brook, New York 11794-3400; ExxonMobil Chemical Company, Baytown, Texas 77522; and ExxonMobil Research and Engineering Company, Annandale, New Jersey 08801

Received January 11, 2004; Revised Manuscript Received April 5, 2004

ABSTRACT: Development of shear-induced crystallization precursor structure was studied by in-situ rheo-SAXS (small-angle X-ray scattering) and rheo-WAXD (wide-angle X-ray diffraction) techniques using binary polymer blends of high and low molecular weight polyethylenes near their nominal melting temperatures (120 °C). Two low molecular weight polyethylene copolymers, containing 2 mol % hexene, with weight-average molecular weights (M_w) of 50 000 (MB-50K) and 100 000 (MB-100K), and polydispersity of about 2, were used as the noncrystallizing matrices. A high molecular weight polyethylene homopolymer with M_w of 250 000 (MB-250K) and polydispersity of about 2 was used as the crystallizing minor component. Two series of model blends, MB-50K/MB-250K and MB-100K/MB-250K, each containing weight ratios of 100/0, 97/3, 95/5, and 90/10, were prepared by solution blending to ensure thorough mixing at the molecular level. At the chosen shear conditions (rate = 60 s^{-1}, duration = 5 s, T = 120 °C), while no flow-induced structures were seen in pure MB-50K and MB-100K melts, the blends in both series showed distinct but different shear-induced structures. Results indicate that the high molecular weight component dominates the formation of crystallization precursor structures in the blend under shear, which can act as a template for further crystallization. A "shish-kebab" structure, detected by both SAXS and WAXD, was observed in the MB-100K/MB-250K (90/10) blend, while only a twisted lamellar structure (kebab) was seen in the rest of the blends under the same shear conditions. These findings suggest that the matrix viscosity plays an important role to influence the formation of crystallization precursor structure of the high molecular component under flow. In the MB-100K/MB-250K (90/10) blend, the length of the shish was estimated from the equatorial streak in SAXS, which showed a noticeable decrease with time, while the corresponding scattering intensity was found to increase. The evolution of the shish-kebab structure from SAXS is consistent with the appearance of the (110) peak in WAXD, which can be explained by the coil−stretch transition induced by flow.

Introduction

Molecular orientation induced by flow during polymer processing operations, such as extrusion, injection molding, fiber spinning, film blowing, etc., can significantly affect the crystallization kinetics and the final polymer morphology.[1−8] As crystalline polymers comprise more than two-thirds of the global polymer production and have a wide range of applications from packaging, textile, automotive components, to biomedical implants, it is essential to understand the exact relationship between structure and processing, particularly at the early stages of crystallization under flow. This is because the initially formed structures often dictate the subsequent development of morphology and thus the final properties.

Despite decades of research on the subject of orientation-induced crystallization, the nature of the earliest events during crystallization under flow has only become available recently with the assistance of advanced characterization tools: (a) in-situ techniques such as rheo-SALS (small-angle light scattering), rheooptical, rheo-SAXS (small-angle X-ray scattering), and rheo-WAXD (wide-angle X-ray diffraction) and (b) ex-situ techniques such as AFM (atomic force microscopy) and TEM (transmission electrical microscopy). We have recently given a brief summary of the flow-induced crystallization studies using these techniques.[9] Among these studies, the role of the long-chain species in flow-induced crystallization has attracted the most attention. For example, using rheooptical methods, Janeschitz-Kriegl et al.[10] reported that in short term shearing at a low degree of supercooling, the crystallization of isotactic polypropylene (iPP) was highly dependent on the content of the long chains. If the long chains were present, shear-induced crystallization was more sensitive to shear treatment and orientation of the surface layers was much higher in these materials. Several other groups, using similar techniques but under different flow conditions, also reported that the presence of long chains strongly affected the crystallization kinetics and the formation of the oriented structure.[11−14] Recently, Kornfield et al.[15] argued that the role of the long chains in shear-induced crystallization is cooperative rather than a single-chain event based on the observation that the oriented structure changed drastically near the overlap concentration of the long chains in binary iPP blends. This certainly makes sense. However, the exact role of the long chains during flow-induced crystallization, i.e., whether the first nuclei are initiated from the long chains or how the long-chain species partake in the crystallization process, remains elusive, which is the purpose of this study.

[†] State University of New York at Stony Brook.
[§] ExxonMobil Chemical Company.
[‡] ExxonMobil Research and Engineering Company.
* To whom correspondence should be addressed: e-mail bhsiao@notes.cc.sunysb.edu; Tel 631-632-7793; Fax 631-632-6518.

10.1021/ma049925f CCC: $27.50
Published on Web 06/05/2004

Our laboratory has studied the flow-induced precursor structures in iPP melt with a broad molecular weight distribution under shear by means of in-situ rheo-WAXD and rheo-SAXS techniques.[9,16−20] Our results support the following pathways for the early stages of flow-induced crystallization in iPP. A "scaffold" (or network) of oriented structures in the supercooled melt is formed under flow prior to the occurrence of full-scale crystallization at lower temperatures. The scaffold structures in the sheared iPP melt contain two components: (1) the primary nuclei (through homogeneous nucleation), which can form the shish structure with long connectivity along the flow direction, and (2) the shish-induced crystalline kebab structure (layered lamellae), which grow perpendicularly to the flow direction but with poor lateral connectivity between the neighboring ones. The fraction of the long chains is thought to be responsible for the formation of primary nuclei in the deformed melt because the stretched long chains can remain anisotropic for a long duration due to their long relaxation times, whereas the shorter chains will relax back rapidly upon the cessation of flow. As the assembly of the oriented chain segments in the long chains can undergo a first-order transition (crystallization or mesomorphic formation in iPP), stable primary nuclei are formed. This argument has been first proposed by Keller and co-workers[5,21−23] using the concept of coil−stretch transition. They proposed the relationship of $\dot{\epsilon}_c \propto (M^*)^{-\beta}$ for the case of elongational flow-induced crystallization in dilute polymer solutions, where $\dot{\epsilon}_c$ is the critical elongational rate, M^* is the critical orientation molecular weight defining the coil−stretch transition, and β is a factor that was found to be equal to 1.5 in polyethylene solution. Only the polymer chains with molecular weights higher than M^* can remain stretched after deformation, while the shorter chains will return to their original coil state. We have also verified the concept of coil−stretch transition for the case of shear flow in polymer melts.[16,17] The observed dependence of M^* on the shear rate was fit to the relationship of $M^* \propto \dot{\gamma}^{-\alpha}$, with α being an exponent and having a value of 0.15 for iPP at 145 °C.

Keller et al.[21−25] and Pennings et al.[26] devoted a great deal of effort to elucidate the development of the shish-kebab morphology under elongational flow from dilute polymer solutions, where the interactions between the polymer molecules were minimized and the behavior of the individual chains was enhanced and examined. Subsequently, extensive studies of the shish-kebab formation in polymer melt under elongational flow and high shear flow were also carried out.[27−36] In comparison with elongational flow, the shear flow is often thought to be a weaker flow, not able to provide sufficient extension to the chains necessary to form the fibrillar structure. However, many experimental results suggest that this consideration is not founded. In several studies, even with the application of relatively weak shear conditions, the overall crystallization kinetics were found to change drastically, and the shish-kebab morphology was observed.[9,37−39] This indicates that the formation of the shish-kebab structure is a local event, depending on the melt dynamics of the chains and the thermodynamics of the structural formation at the submicron scales, instead of the properties in the bulk state. In a recent review by Keller and Kolnaar, they also argued that although the full extension of the chains in shear was unlikely, the extension of portions of the chain was still possible, which could form the basis for the shish-kebab structure.[5]

The formation of the flow-induced shish structure is related to homogeneous nucleation of oriented chains (the transition is initiated from a single phase). The process of homogeneous nucleation from a single chain or a few interacting chains has been demonstrated by the simulation works of Muthukumar et al.[40−44] The major physical characteristics of their simulations are consistent with the experimental observations at the quiescent state. Recently, they further demonstrated that the development of the shish-kebab morphology is related to the coil−stretch transition of isolated chains under extensional flow.[44] Even for monodisperse chains, the calculated free energy landscape shows that two populations of stretched and coiled conformations are formed at a given flow rate. The stretched chains can crystallize into shish, while the coiled chains can adsorb onto the shish and transform into the lamellae (kebabs). The local inhomogeneity in polymer concentration and the change of flow rate can significantly alter the population of stretched and coiled conformations, thus affecting the onset of shish-kebab morphology. In a different simulation effort, Hu et al.[45] have also demonstrated that a single oriented chain can induce transcrystallization, which implies that the lowest limit of the shish diameter is the stem of a single chain. It is conceivable that the actual shish entity induced by flow consists of an assembly of oriented chain segments. If the dimensions (diameter and length) of the shish are too small and/or the concentration of the shish is too dilute, their presence may not be able to be detected by even the advanced characterization techniques such as synchrotron SAXS with high sensitivity. (In this study, we thus only discuss the shish structures as those that can be detected by synchrotron SAXS.) This raises an interesting question about the factors that can influence the formation of shish. Obviously, these factors include the material characteristics (such as molecular weight, molecular weight distribution, chain architecture: linear or branch, etc.) and shear conditions (such as shear rate, shear strain, and temperature).

In this study, a unique polymer blend system, inspired by Keller and co-workers' studies on dilute polymer solutions under flow,[21−25] was used to simulate the formation of precursor structures at the early stages of flow-induced crystallization. In these blends, two low molecular weight polyethylene (PE) samples were used as the "solvent" or the matrix material of different viscosity (their molecular weights were significantly higher than the molecular weight between the entanglements for PE $\sim$ 1250 g/mol[46]); the high molecular weight polyethylene (MB-250K) that is miscible with both low molecular weight polyethylene matrices[47,48] was used as the crystallizing component in the model blends. In addition, we have identified two specific requirements for the selection of the experimental conditions. (1) The matrix should be kept amorphous during the experiment as in the "dilute polymer solution" condition, allowing the examination of only the crystallization behavior of the high molecular weight component under shear. (2) The crystallization kinetics of the high molecular weight species in the blends must be sufficiently slow (this can be adjusted by the crystallization temperature), allowing the real-time measurements by synchrotron SAXS and WAXD studies (the transition period should be in minutes instead of seconds). To meet

Table 1. Polyethylene Sample Information

sample	M_w (g/mol)	M_w/M_n	T_m (°C)	$T_{m,end}$ (°C)	hexene (mol %)	crystallinity (%)[b]
MB-50K	~50 000	~2	112	119.8	2	31.9
MB-100K	~100 000	~2	117	120.8	2	32.7
MB-250K[a]	~250 000	~2	127	131		54.3

[a] The density of MB-250K was 0.92 g/cm^3. [b] Crystallinity $X_C = \Delta H_f(T_m)/\Delta H_f°(T_m°)$. $\Delta H_f°(T_m°)$ represents the enthalpy of fusion of a completely crystalline sample measured at the equilibrium melting point ($T_m°$). $\Delta H_f°(T_m°)$ for polyethylene is 293 J/g.

both requirements, the following steps were taken: (A) Two lower molecular weight ethylene−hexene copolymers (50 000 and 100 000 g/mol) were chosen as the matrix materials (composition in the blend >90 wt %), having a lower melting point, lower crystallinity, and slower crystallization kinetics than those of the high molecular weight minor component (a linear PE "homopolymer" with M_w of 250 000 g/mol). All samples were made by the metallocene catalyst process, having a well-defined polydispersity of about 2. (B) The experimental temperature was carefully chosen on the basis of the following considerations. In our earlier study of iPP,[9] the temperature window for observing the flow-induced precursor structures at the very early stages of crystallization was found to be relatively narrow. In other words, no precursor structures can be detected if the experimental temperature is too high. On the other hand, if the temperature is too low, the rapid crystallization growth will overwhelm the precursor structures. The chosen blends have significantly simplified the temperature selection process. The experimental temperature was chosen near the end of the melting zone ($T_{m,end}$ in DSC thermogram) of the low molecular weight component, where the low molecular weight matrix would stay amorphous but the high molecular weight component could be readily crystallized and studied. (C) The selected concentrations of the binary blends were above the overlap concentration, C^*. This concentration range could be used to simulate the practical molecular weight distribution in common polymers. The above experimental conditions (A−C) allowed us to clearly study the crystallization behavior of the long-chain component in the shear melt since the short-chain copolymer matrix would not partake in the formation of the flow-induced structures.

2. Experimental Section

2.1. Sample Preparation. The chosen polyethylene samples were experimental grade polyethylene samples synthesized particularly for this project at the ExxonMobil Research and Engineering Co., Annandale, NJ. The sample information such as molecular weights, polydispersity, compositions, nominal melting temperature, end melting temperature ($T_{m,end}$ from DSC), and crystallinity are shown in Table 1. The chosen low molecular weight matrix samples (MB-50K and MB-100K) were copolymers of ethylene and hexene (2 mol %), having lower values of crystallinity and slower crystallization rates when compared to their homopolymer counterparts of the same molecular weight. The high molecular weight sample (MB-250K) was considered a "homopolymer", even though it might contain a small amount of hexene comonomer. This is because its melting and crystallization behavior was very similar to that of a linear homopolymer without the comonomer unit. These model samples, all prepared by a metallocene catalyst reaction, were used to prepare the binary polyethylene blends with varying concentrations of the high molecular weight component.

Polymer blends were prepared by the solution blending to ensure the intimate mixing of different species at the molecular level. The blending procedures were as follows. The mixture of low molecular weight PE, high molecular weight PE, and antioxidant agent (Irgonox 1076) were first dissolved in xylene to form a homogeneous solution. The typical polymer concentration was 2.8 wt % in the solution, and the weight percentage of Irgonox 1076 was 5 wt % in the total polymer blend. The mixture was heated slowly under vigorous stirring until the polymers were completely dissolved in xylene (the solution became transparent). The homogeneous solution was held at 120 °C for 60 min with continuous stirring. Precipitation of the polymer blends was carried out by pouring the polymer solution into cold methanol (5−6 times the original volume of xylene in the polymer solution) under continuous stirring. The polymer blend slurry was then filtered from a xylene and methanol mixture and vacuum-dried at 80 °C for at least 2 days. As a substantial amount of antioxidant agents might be lost during the washing process, additional 2 wt % of Irgonox 1076 was added to the recovered polymer blend powder to avoid the degradation of the polymers during compression molding. Control samples of two pure low molecular weight polyethylenes without the addition of the high molecular weight component were also prepared as reference materials using the same procedure as for the blends. The compositions of the prepared blends are summarized in Table 2. The overlap concentration[49] for both MB-50K/MB-250K and MB-100K/MB-250K blends, based on the published data for 250K linear PE (i.e., the ratio of radius of gyration and M_w is 0.208[50]), was about 1 wt %. Thus, all chosen concentrations of the binary blends (3, 5, and 10 wt %) were above the overlap concentration. Polymer films of 0.5−0.7 mm thickness were prepared by compression molding at 150 °C. Samples in the form of a ring (inner diameter = 10 mm, outer diameter = 20 mm) were cut from the molded films for shear experiments.

Table 2. Polyethylene Model Blends Compositions

blends	wt % of low-M_w PE	wt % of high-M_w PE
MB-50K/MB-250K (100/0)	100	0
MB-50K/MB-250K (97/3)	97	3
MB-50K/MB-250K (95/5)	95	5
MB-50K/MB-250K (90/10)	90	10
MB-100K/MB-250K (100/0)	100	0
MB-100K/MB-250K (97/3)	97	3
MB-100K/MB-250K (95/5)	95	5
MB-100K/MB-250K (90/10)	90	10

2.2. Instrumentationand Experimental Procedures. DSC measurements were carried out to characterize the thermal properties of the blends using a Perkin-Elmer DSC 7 instrument. The sample pans were hermetically sealed. The DSC scan was calibrated with the indium standard. Typically, 6−8 mg samples were used in each DSC run. In the first scan, the sample was heated from 30 to 160 °C, held there for 3 min, and subsequently cooled to 30 °C, both at the rate of 10 °C/min. After the first scan, the second scan was obtained during heating to 160 °C at 10 °C/min. All DSC scans were carried out under a nitrogen environment.

Two-dimensional (2D) wide-angle X-ray diffraction (WAXD) and small-angle X-ray scattering (SAXS) measurements (not measured simultaneously) were carried out at the X3A2 synchrotron beamline in the National Synchrotron Light Source (NSLS), Brookhaven National Laboratory (BNL). The wavelength of the synchrotron radiation was 1.54 Å. The shear stage was placed perpendicular to the incident X-ray beam. 2D WAXD and SAXS patterns were collected by means of a MAR CCD X-ray detector (MARUSA) with a resolution of 1024 × 1024 pixels (pixel size = 158.44 μm). The sample-to-detector

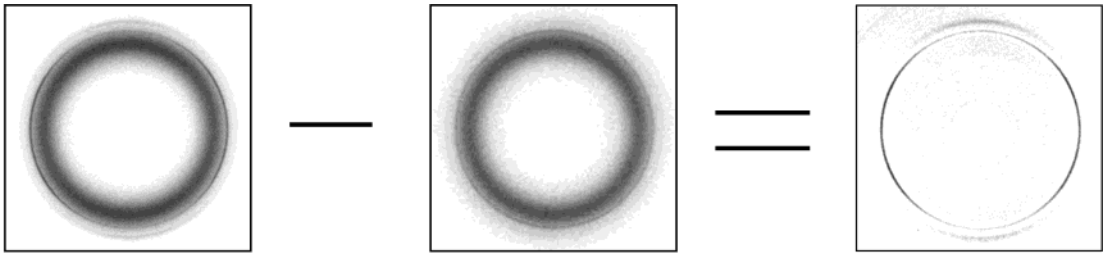

Figure 1. Example of 2D WAXD image analysis using the "halo" methods. The three chosen images represent the MB-100K/MB-250K (90/10) blend at 1475 s after shear cessation: the corrected total scattered intensity (left), isotropic scattered intensity (unoriented crystals and amorphous) (middle), and oriented scattered intensity (right).

distance was 106 mm in WAXD and 1610 mm in SAXS. The experimental setup of the synchrotron beamline and the placement of the shear stage were given in previous publication.[16] The SAXS angle was calibrated with AgBe (silver behenate), and the WAXD angle was calibrated with Al_2O_3 (aluminum oxide) standard. All images were normalized for beam fluctuations and sample absorption.

A Linkam CSS-450 high-temperature shear stage modified for in-situ X-ray scattering measurements was used to control the shear conditions of the polymer samples. A diamond window and a Kapton film were used in place of two standard quartz optical windows on the top and bottom of the steel blocks in the Linkam stage. The details of this modified shear apparatus have been described elsewhere.[16] The sample was placed in the gap between the two X-ray windows. Shear was applied to the sample by rotating the bottom window while keeping the top window stationary. The mechanical design and electronics of the Linkam stage provided precise control over the various parameters of the shear experiments, including sample thickness, temperature, heating/cooling rate, shear rate, shear strain and duration, as well as the shear mode such as steady, step, and oscillatory.

In each experiment, the polymer sample was mounted between the two X-ray windows. The gap between the two windows defined the sample thickness. To ensure that the polymer melt was free of any memory effects associated with clusters or crystal aggregates due to the prior temperature and deformation, all polymer samples were subjected to the following thermal protocol. The samples were first heated to 165 °C (which is above the equilibrium melting point of polyethylene, $T_m° \sim 145.5$ °C) and were held there for 5 min. The equilibrated melt was then cooled to the chosen crystallization temperature at a 30 °C/min rate. Once the temperature reached the chosen experimental temperature, a WAXD (or SAXS) pattern was collected before the shear was applied. Time-resolved X-ray images were then subsequently taken upon the cessation of shearing. The acquisition time for each image was 10 s with an interval of 5 s for data transfer between the adjacent images. The program was set to collect 180 consecutive X-ray images. In each run, an air scattering pattern with no sample between the two windows of the shear stage was also collected. The background correction of the WAXD and SAXS images was performed to eliminate the air scattering background. All X-ray images were also normalized for the sample thickness and the beam fluctuations. The analysis of the X-ray data was carried out using the corrected patterns.

3. X-ray Data Analysis

3.1. WAXD. It is well-known that the scattered intensity from a partially oriented sample usually contains two contributions: (1) the isotropic part due to the amorphous phase and unoriented crystals and (2) the anisotropic part due to the oriented crystals. The total crystallinity thus can be separated into two fractions due to unoriented and oriented crystals. To accomplish this, we first deconvolute the total scattering into two contributions from oriented and unoriented parts, using the "halo" method, which has been described elsewhere.[51] The principle of this deconvolution method is outlined briefly below. The azimuthally independent component in the total scattered intensity is directly proportional to the unoriented fraction of the material,[16] which can be determined as follows. For each azimuthal scan at a specific 2θ angle, the minimum value of the intensity profile can be considered as the envelope intensity of the unoriented species at that scattering angle. By extracting all the minimum values for all the scattering angles, a 2D image of the isotropic contribution (that includes the amorphous phase and unoriented crystals) can be generated. This isotropic contribution can then be subtracted from the total scattering image, yielding the oriented contribution only.

Figure 1 illustrates the initial 2D WAXD pattern (after correction for air scattering, sample absorption, and beam fluctuations) of MB-100K/MB-250K (90/10) blend obtained at 1475 s after shear and the deconvoluted 2D images of isotropic and oriented contributions obtained after the above analysis. Circularly averaged linear intensity profiles from the corrected 2D WAXD pattern and the extracted isotropic contribution are shown in parts A and B of Figure 2, respectively. A one-dimensional peak-fit routine was further used to deconvolute the peaks in the linear intensity profiles, using a procedure outlined below. For the total scattered intensity, the shape of the amorphous peak was obtained from the WAXD pattern of the amorphous polymer melt collected before shear, which was fitted with three Gaussian functions. Two additional Gaussian functions were used to fit the crystalline peaks (110 and 200). The peak parameters such as height, width, and area of each crystal reflection were obtained after the iterative peak-fitting procedure. The total crystallinity index was estimated by subtracting the area percentage of the amorphous phase from 100%

$$X_C^T = 100\% - X_A^T \quad (1)$$

with X_C^T being the total crystallinity index and X_A^T being the area percentage of the amorphous phase

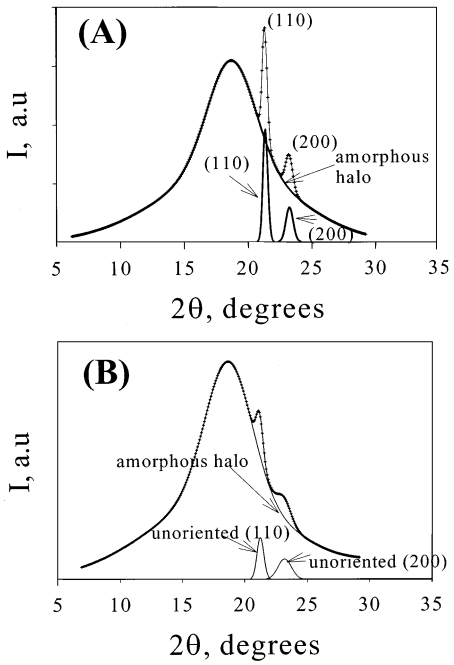

Figure 2. Deconvolution of peaks in the total WAXD intensity profile (A) and the unoriented WAXD intensity profile (B) (data were from Figure 1).

from the total scattering profile. The superscript "T " represents the total scattering. We note that the crystallinity index (termed "crystallinity" from here on) estimated this way was different from the true crystallinity. This is because the measured 2D WAXD pattern was partially oriented, where the circular averaging did not result in an undistorted scattered intensity profile.

From the isotropic intensity profile (Figure 2B), the fraction of unoriented crystals was estimated using a similar peak-fit procedure. During fitting, the shape and position of the amorphous peak were kept constant as the deconvolution of the total scattered intensity, while the height was allowed to change. On the basis of this procedure, the ratio of the unoriented crystal fraction and the amorphous fraction, R, was calculated

$$R = X_{UC}{}^{U}/X_{A}{}^{U} \tag{2}$$

with $X_{UC}{}^{U}$ and $X_{A}{}^{U}$ being the fractions of unoriented crystals and amorphous phase estimated from the unoriented WAXD profile. We note that $X_{A}{}^{U}$ was different from $X_{A}{}^{T}$ (the value of $X_{A}{}^{U}$ was bigger than $X_{A}{}^{T}$), which was due to the procedure of circular averaging. To estimate the crystallinity of unoriented crystals in reference to the total scattered intensity ($X_{C}{}^{T}$), we applied the ratio R calculated from eq 2, which keeps constant in both total scattering and unoriented scattering WAXD files, to $X_{A}{}^{T}$ (i.e., the presence of oriented amorphous phase in PE is negligible). The following equation was used:

$$X_{UC}{}^{T} = X_{A}{}^{T}R \tag{3}$$

Thus, the crystallinity of oriented crystals in reference to the total scattering could be calculated as

$$X_{OC}{}^{T} = X_{C}{}^{T} - X_{UC}{}^{T} \tag{4}$$

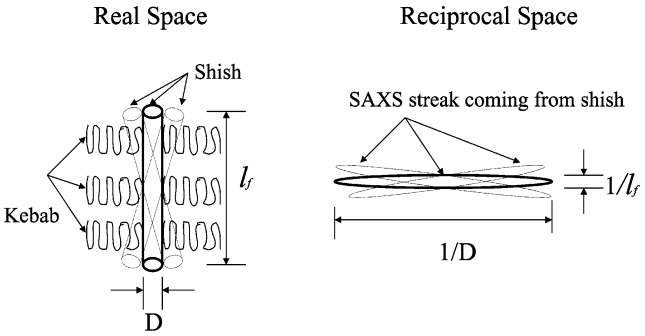

Figure 3. Schematic diagram of scattering in reciprocal space due to crystal fibril of length, l_f, in real space.[50]

The oriented fraction in the crystalline phase (F) was calculated using the following equation:

$$F = X_{OC}{}^{T}/X_{C}{}^{T} \tag{5}$$

3.2. SAXS. The "kebab" information was determined as follows. Linear intensity profiles along the meridian as a function of the scattering angle (2θ) or q ($= 4\pi \sin \theta/\lambda$) were extracted from the 2D SAXS patterns. Lorentz corrections were carried out for these profiles (the scattered intensity was multiplied by q^2) in order to correct the slight misorientation of lamellar structure.[52] The peak position of the scattering maximum (q_{max}) in the Lorentz-corrected plot was used to determine the average spacing ($L = 2\pi/q_{max}$) between the adjacent lamella stacks (or kebabs) along the meridian (i.e., the shear direction). In our previous publication,[20] these procedures have been described in detail.

To determine the shish information observed in the sheared MB-100K/MB-250K (90/10) blend, the following procedures were taken. A method proposed by Ruland[53] was used to analyze the intensity distribution of the "streak" along the equator of SAXS pattern. The analysis can give information about the average length of the shish (or microfibrils) and its misorientation from the fiber axis, which has recently been successfully applied by us to investigate the microstructure changes during deformation of Kevlar fibers.[54] A schematic diagram of the relationship between the scattering streak along the equator in reciprocal space and the fibril of length l_f in real space is shown in Figure 3. In this diagram, the length of the streak along the equator corresponds to $1/D$ of the fibril, where D is the diameter of the fibril; the width of the streak in reciprocal space corresponds to $1/l_f$ of the fibril in real space. A series of azimuthal scans at different q (or $s = 2\pi/q$) values along the equator were performed and fitted with a Lorentzian function. (The Lorentzian function gave a better fit than the Gaussian function.) The integral breadth (B_{obs} = peak area/peak height) of each azimuthal profile was determined as a function of s. The following equation[53] represents the relationship between the fibril length and its misorientation width, B_ϕ:

$$B_{obs} = \frac{1}{l_f}\frac{1}{s} + B_\phi \tag{6}$$

Thus, l_f can be obtained from the slope of B_{obs} vs $1/s$ plot, and the intercept gives the misorientation width.

4. Results

4.1. Rheo-WAXD. Figure 4 shows selective 2D WAXD patterns of MB-50K/MB-250K (95/5) blend (A) and MB-

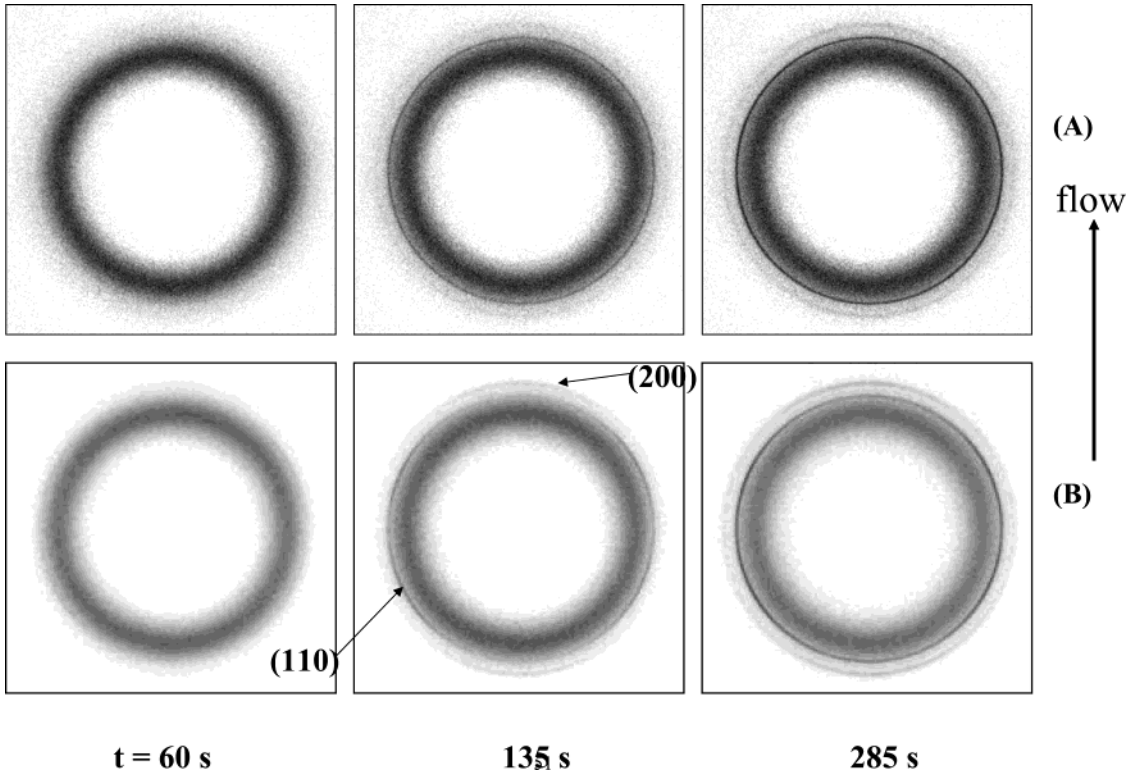

Figure 4. Selected 2D WAXD patterns of (A) MB-50K/MB-250K (95/5) and (B) MB-50K/MB-250K (90/10) after shear cessation.

50K/MB-250K (90/10) blend (B) at different times after cessation of shear (shear rate = 60 s^{-1}, shear time = 5 s, T = 120 °C). The flow direction is vertical. Only patterns collected at early stages are shown here, since the precursor structures in the early stages of the crystallization are of particular interest. The patterns at the later stages are very similar to the last image (285 s) shown in Figure 4, only with higher intensity.

Before we discuss the details of the changes in the observed patterns, it is necessary to first describe results (not shown here) from pure MB-50K polymer (the matrix) with and without shear and the MB-50K/MB-250K blends (95/5 and 90/10) without shear at the same temperature. These results are important reference points to confirm the validity of our experimental design, which are summarized as follows. (1) All WAXD patterns of pure MB-50K melt with and without shear showed a completely diffuse scattering pattern with no indication of crystal reflections during the experimental time frame (up to 2685 s). Clearly, pure MB-50K polyethylene melt did not crystallize at the chosen experimental temperature (120 °C), with and without shear. (2) WAXD patterns from both MB-50K/MB-250K blends (95/5 and 90/10) under no shear showed the occurrence of crystallization at a time around 165 s. Two crystal reflections, which could be indexed as (110) at 2θ = 21.6° and (200) at 2θ = 23.1°, were seen, but neither exhibited any orientation. The crystalline feature resulted mainly from the entity of MB-250K homopolymer as expected. The blend with the higher concentration of MB-250K (90/10) showed a higher crystallinity but with a similar crystallization rate.

Prior to shear, the initial WAXD patterns (t = 0) of both MB-50K/MB-250K (95/5) and (90/10) blends showed an amorphous ring, confirming the thermal clearing of all residual crystalline structures in the melt before the experiment. In Figure 4, no crystal reflections could be detected in the WAXD pattern of MB-50K/MB-250K (95/5) blend at t = 60 s after shear, while the corresponding pattern of MB-50K/MB-250K (90/10) blend clearly showed four weak (110) peaks at off-axis locations. In the MB-50K/MB-250K (95/5) blend, the crystal reflections were first seen at around 135 s after shear. All observed crystal reflections in the sheared blends were anisotropic, i.e., azimuthal variations in the intensity, indicating crystal orientation. It was further found that the degree of orientation was stronger in the MB-50K/MB-250K (90/10) blend than the (95/5) blend. In the WAXD pattern of MB-50K/MB-250K (90/10) blend at 135 s after shear, four (110) reflections in the form of arcs at the off-axis direction and two (200) reflections in the meridian were seen. The appearance of four-arc off-axis (110) reflections and two-arc meridional (200) reflections is an indication of twisted lamellae,[5,55] which will be discussed later. With the increase of time, the crystalline reflections grew stronger, but the crystal orientation decreased continuously. The strongest crystal orientation was observed in the initial few patterns after shear. We note that the WAXD patterns obtained for MB-50K/MB-250K (97/3) blend (not shown here) were very similar to those of the MB-50K/MB-250K (95/5) blend, except that its crystallization started at a slightly later time.

Figure 5 shows selective 2D WAXD patterns of MB-100K/MB-250K (95/5) blend (A) and MB-100K/MB-250K (90/10) blend (B) at different times after shear (shear rate = 60 s^{-1}, shear time = 5 s, T = 120 °C). As discussed earlier, experiments of pure MB-100K polymer with shear and without shear as well as the MB-100K/MB-250K (90/10) blend without shear were first carried out to check the experimental conditions. WAXD measurements of the MB-100K/MB-250K (90/10) blend under no shear showed that crystallization (of the MB-100K phase) began at about 285 s without any detectable crystal orientation, which was slower than that for the MB-50K/MB-250K (90/10) blend. The difference

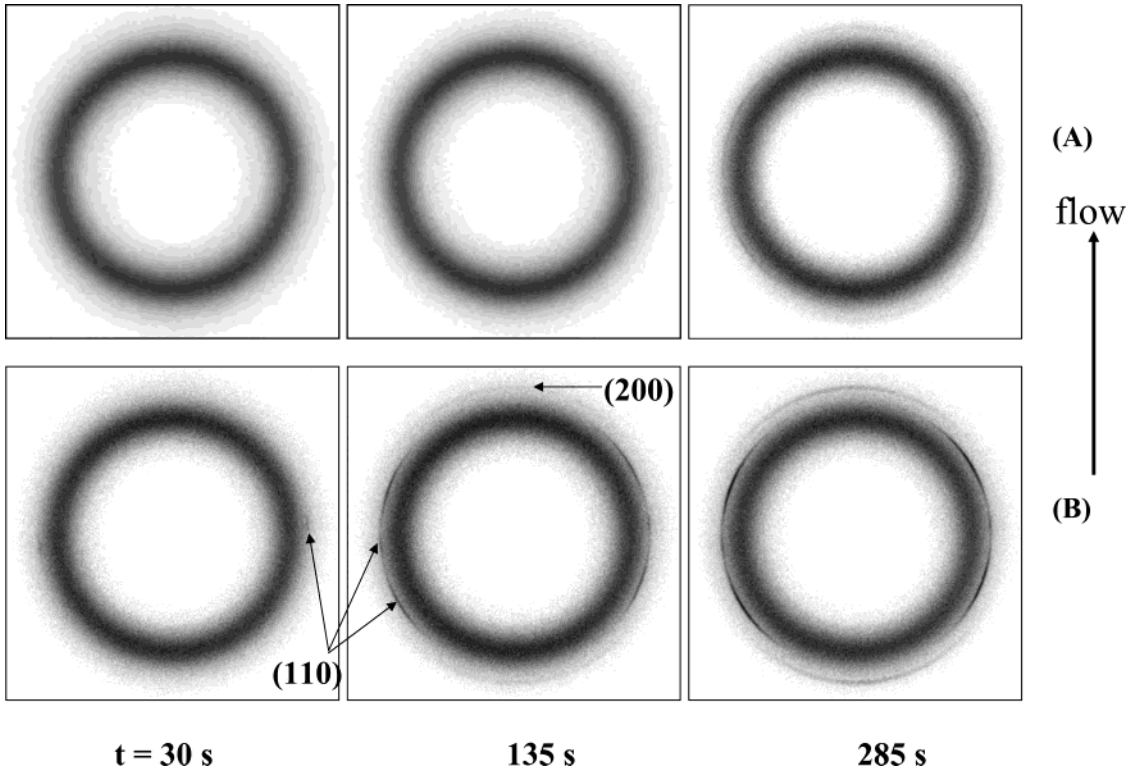

Figure 5. Selected 2D WAXD patterns of (A) MB-100K/MB-250K (95/5) and (B) MB-100K/MB-250K (90/10) after shear cessation.

must be due to the effect of the matrix mobility, which will be discussed later. Similar to the observations in Figure 4, both blends showed that crystal orientation and crystallization kinetics increased significantly after shear with the increase in the MB-250K concentration. The overall behavior of the MB-100K/MB-250K (95/5) blend (Figure 5A, as well as the MB-100K/MB-250K (97/3) blend not shown here) was quite similar to that of the MB-50K/MB-250K blends, except that a slower crystallization rate (the crystallization started at around 235 s after shear) was observed than that of its counterparts (MB-50K/MB0250K).

In contrast, the WAXD pattern of the MB-100K/MB-250K (90/10) blend obtained immediately after shear (∼30 s) showed a very unique feature, different from the one previously observed in the other blends. It was found that a pair of sharp (110) reflections appeared almost immediately upon the cessation of flow on the equator. (The earlier patterns showed the occurrence of four (110) reflections at the off-axis positions.) The formation of this equatorial two-spot pattern at the very early stages of crystallization indicates that the first formed crystals had a very high orientation, and the chains in the formed crystals were aligned parallel to the flow direction. Subsequent crystallization in the sheared MB-100K/MB-250K (90/10) blend led to a composite pattern having six (110) reflections and two (200) reflections in the meridian (as seen the 135 and 285 s SAXS patterns in Figure 5B).

4.2. Crystallinity Development in Different Matrix. Time evolution of the total crystallinity for the two blend series MB-50K/MB-250K (100/0, 97/3, 95/5, and 90/10) and MB-100K/MB-250K (100/0, 93/7, 95/5, and 90/10) is illustrated in parts A and B of Figure 6, respectively. It was seen that the total crystallinity level was always lower than the weight percentage of MB-250K linear polymer, and the crystallinity of the two low molecular weight matrices (MB-50K and MB-100K) was zero during the experimental time period (∼45 min). These findings confirmed that the observed crystallization behavior resulted mainly from the transition in the MB-250K component, which exhibited different kinetics in a different matrix. In Figure 6a, all MB-50K/MB-250K blends show a relatively fast crystallization behavior immediately after shear. The final values of the total crystallinity at the end of the measurements were approximately 2.8, 4.8, and 6.2% for 97/3, 95/5, and 90/10 blends, respectively. The 3 wt % blend exhibited the slowest crystallization kinetics among the chosen three compositions. A similar behavior was also seen in MB-100K/MB-250K blends (Figure 6b). The final values of the total crystallinity in the MB-100K/MB-250K blends were approximately 2.3, 4.7, and 5.3% for 97/3, 95/5, and 90/10 blends, respectively. Compared to MB-50K/MB-250K blends, the MB-100K/MB-250K blends showed notably slower kinetics at the same experimental conditions.

Figure 7 illustrates the crystallization half time ($t_{1/2}$) for the MB-250K component in different blends at the chosen experimental conditions (shear rate = 60 s^{-1}, shear time = 5 s, T = 120 °C). The crystallization half-time was determined from the time evolution curve of the total crystallinity (Figure 6) using the following procedures. At $t = 0$, the value of the total crystallinity, X_C^T (0), is zero. The difference, $X_C^T(t) - X_C^T(0)$, represents the rise in the total crystallinity, and $X_C^T(s)$ is the final value of the total crystallinity. Thus, the total crystals fraction (f) at a certain time can be defined as follows:

$$f(t) = [X_C^T(t) - X_C^T(0)]/[X_C^T(s) - X_C^T(0)] \qquad (7)$$

The half-time, $t_{1/2}$, was taken as the time corresponding to $f = 0.5$. It is seen in Figure 7 that the crystallization half-time value of MB-250K in the MB-50K matrix is less than that in the MB-100K matrix at the same

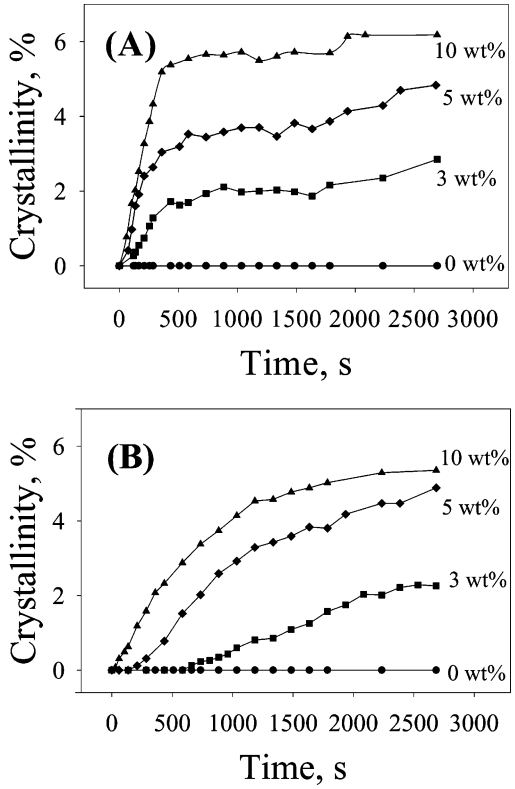

Figure 6. Evolution of the total crystallinity in (A) MB-50K/MB-250K (100/0, 93/7, 95/5, and 90/10) blends and (B) MB-100K/MB-250K (100/0, 93/7, 95/5, and 90/10) blends after shear as a function of time.

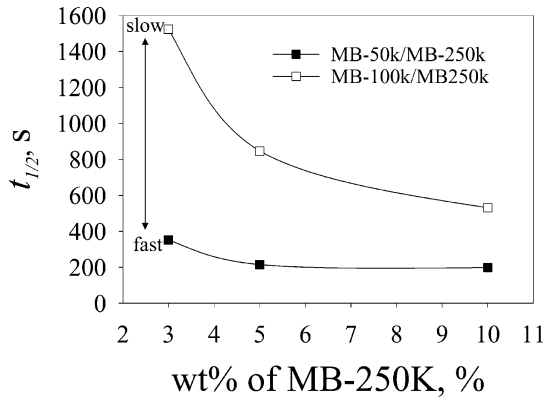

Figure 7. Concentration effect of high molecular weight component (MB-250K) on the half-time of crystallization in MB-50K/MB-250K and MB-100K/MB-250K blends series.

concentration level. Furthermore, the crystallization half-time value decreased with the increase in MB-250K concentration. (The $t_{1/2}$ decrease in MB-100K/MB-250K was particularly significant.) These results indicate that the viscosity of the medium (as a function of molecular weight and concentration) plays an important role in facilitating the crystallization of MB-250K. As the viscosity is high (higher molecular weight matrix and higher solute concentration), the transportation of the crystallizing chains is slower, thus resulting in slower crystallization kinetics.

4.3. Evolution of Oriented Crystals. During the step-shear experiment, the flow-induced crystallinity consists of two contributions: (1) the oriented crystals, initiated from the stretched MB-250K chains, and (2) the unoriented crystals, resulting mainly from the unstretched MB-250K chains. The development of the

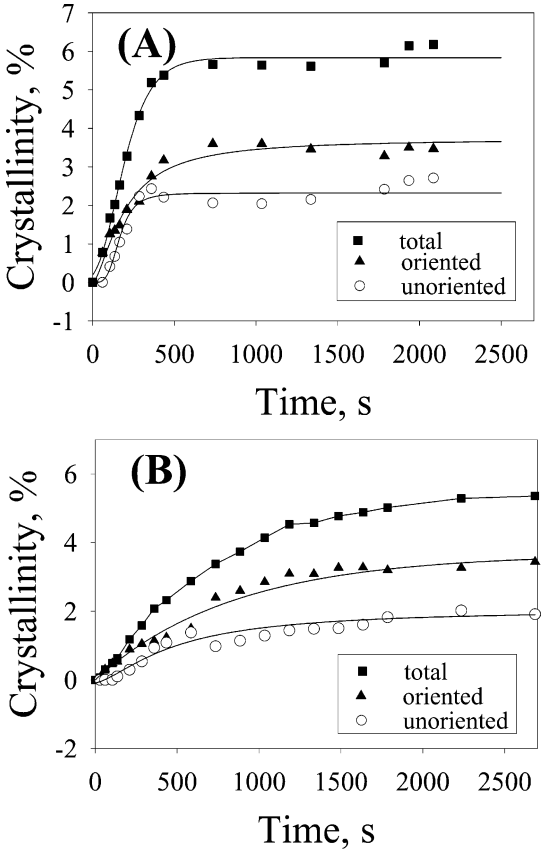

Figure 8. Development of the total crystallinity and crystallinity due to oriented and unoriented fractions in (A) MB-50K/MB-250K (90/10) and (B) MB-100K/MB-250K (90/10) blends after shear.

oriented crystals in (1), containing both stretched and unstretched chains,[44] is of particular interest as it reflects the state of the chains from two different populations (stretched and unstretched), both partaking in the crystallization process. Since the highest concentration (90/10) blends in both MB-50K/MB-100K and MB-100K/MB-250K series showed the strongest crystal orientation after shear, the development of the oriented crystals in these two blends is discussed below. The crystallinity due to the oriented and unoriented crystals was obtained using the WAXD data analysis procedures outlined earlier. The time evolution profiles of the total crystallinity and the crystallinity due to oriented and unoriented crystals for MB-50K/MB-250K (90/10) and MB-100K/MB-250K (90/10) blends are illustrated in parts A and B of Figure 8, respectively. As expected, the total crystallinity developed at a faster rate in the MB-50K/MB-250K (90/10) blend than in the MB-100K/MB-250K (90/10) blend after shear. It is interesting to note that the oriented crystals also grew faster in the MB-50K/MB-250K (90/10) blend than in the MB-100K/MB-250K (90/10) blend. In the early stages of crystallization, the oriented crystallinity was found to be very close to the total crystallinity, indicating that most of the initial crystals were formed from the stretched polymer chains. The unoriented crystal evolution profiles for both blends showed that the unoriented crystals began to develop at a later time after the occurrence of oriented crystals.

Figure 9 illustrates the plot of oriented crystal fraction, F, as a function of crystallization time for the MB-50K/MB-250K (90/10) (filled symbols) and MB-100K/MB-250K (90/10) (unfilled symbols) blends. In the early

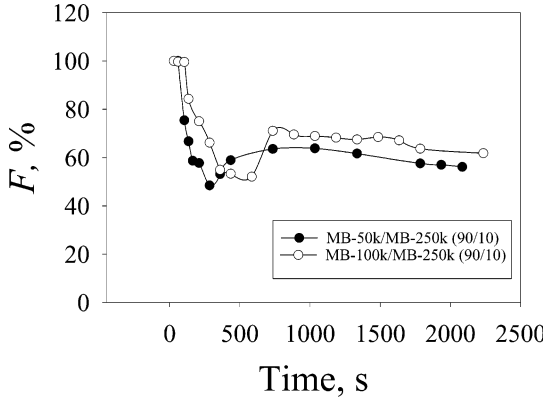

Figure 9. Evolution of the fraction of oriented crystals in MB-50K/MB-250K (90/10) and MB-100K/MB-250K (90/10) blends after shear.

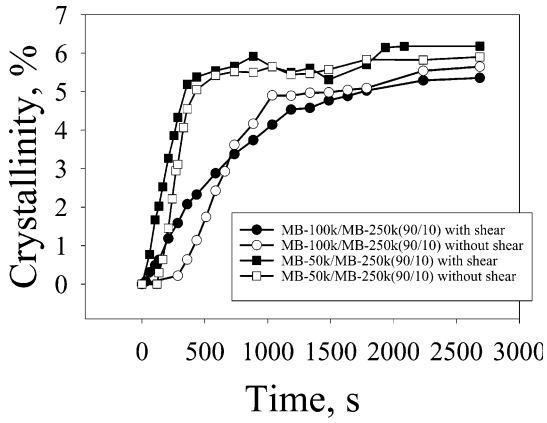

Figure 10. Evolution of the total crystalline phase in MB-50K/MB-250K (90/10) and MB-100K/MB-250K (90/10) blends under shear and no shear condition.

stages of crystallization, immediately after shear, the initial values of the oriented crystal fraction for both MB-50K/MB-250K (90/10) and MB-100K/MB-250K (90/10) blends were very high (~100%), but they decreased rapidly with time. The decrease of F in MB-50K/MB-250K (90/10) was faster than that in MB-100K/MB-250K (90/10), indicating that the unoriented crystals in MB-50K/MB-250K (90/10) developed at a faster rate at the early stages of crystallization. It was interesting to note that the rapid decrease in F stopped at a certain time, and the F value started to increase and then decreased again, exhibiting a minimum value in both blends. The minimum F value was found at 285 s for the MB-50K/MB-250K (90/10) blend and at 585 s for the MB-100K/MB-250K (90/10) blend. Our interpretations of this unusual behavior are presented in the Discussion section. Finally, the near plateau value of the oriented crystal fraction in the MB-100K/MB-250K (90/10) blend was higher than that in the MB-50K/MB-250K (90/10) blend.

4.4. Effect of Shear on Crystallization Kinetics. It is well-known that shear flow can significantly change the crystallization kinetics and influence the final morphology of the polymer.[1,9,10] Figure 10 compares the time evolution curves of the total crystallinity after shear and under no shear in the MB-50K/MB-250K (90/10) and MB-100K/MB-250K (90/10) blends. The corresponding values of the crystallization half-time are also summarized in Table 3. It was found that the effect of shear on the crystallization kinetics (Figure 12) was notable only at the early stages of crystallization. For

Table 3. Half-Time of Crystallization ($t_{1/2}$) in MB-50K/MB-250K (90/10) and MB-100K/MB-250K (90/10) under Quiescent and Shear Conditions at 120 °C

	$t_{1/2}$, s	
sample	shear	quiescent
MB-50K/MB-250K (90/10)	198	271
MB-100K/MB-250K (90/10)	531	682

instance, in the MB-50K/MB-250K (90/10) blend, crystallization under no shear exhibited a delay of about 135 s in the induction time compared to that under shear. Similarly, the induction time for crystallization under no shear exhibited a delay of about 285 s in the MB-100K/MB-250K (90/10) blend. Afterward, crystallization under shear and no shear exhibited a similar behavior for both blends. Although the overall crystallization rate (inversely proportional to the crystallization half-time) was slightly lower under no shear than that under shear for both blends, the crystal growth (slope) and the final values of the total crystallinity obtained under shear and no shear were very close to each other. In fact, in the quiescent MB-100K/MB-250K (90/10) blend, its total crystallization rate was higher than that under shear, and the final total crystallinity was also higher. Accordingly, these results indicate that the shear field mostly affected the induction time or the early stages of crystallization and had a small effect on the overall crystallization rate as well as the final crystallinity in these two model blends.

4.5. Rheo-SAXS. Figure 11 shows 2D SAXS patterns of (A) MB-50K/MB-250K (95/5) and (B) MB-50K/MB-250K (90/10) blends at selected times after shear (shear rate = 60 s^{-1}, shear time = 5 s, T = 120 °C). As a reference, pure MB-50K polymer under shear and no shear, as well as the MB-50K/MB-250K (90/10) blend under no shear, were also studied. Consistent with the WAXD results, SAXS patterns of pure MB-50K matrix did not show any crystallization or orientation features under shear or no shear. SAXS patterns of the MB-50K/MB-250K (90/10) blend under no shear exhibited a diffuse ring with scattering maximum but no orientation. The ring pattern was due to the formation of a randomly oriented lamellar structure. These observations were consistent with the observed WAXD results.

In SAXS patterns of the sheared MB-50K/MB-250K (95/5) blend (Figure 11A), a pair of weak scattering maxima along the flow direction first emerged at around 135 s after shear. Subsequently, these oriented features grew stronger with time. On the other hand, relatively intense meridional scattering peaks were seen almost immediately after shear (<30 s) in the MB-50K/MB-250K (90/10) blend that also grew rapidly with time after shear. The meridional scattering maxima in the SAXS pattern can be attributed to the kebab-like lamellar crystals that are oriented perpendicularly to the flow direction. No other scattering features (such as equatorial streak) were observed in MB-50K/MB-250K (95/5) or MB-50K/MB-250K (90/10) after shear. The absence of the equatorial streak does not necessarily mean that the shish nuclei do not form; they are probably just too small to be detected by SAXS. A similar behavior was observed in our recent studies with isotactic polypropylene.[10,18,20]

Figure 12 shows 2D SAXS patterns of (A) MB-100K/MB-250K (95/5) and (B) MB-100K/MB-250K (90/10) blends at selected times after shear (shear rate = 60 s^{-1}, shear time = 5 s, T = 120 °C). Again, SAXS measurements of pure MB-100K polymer under shear

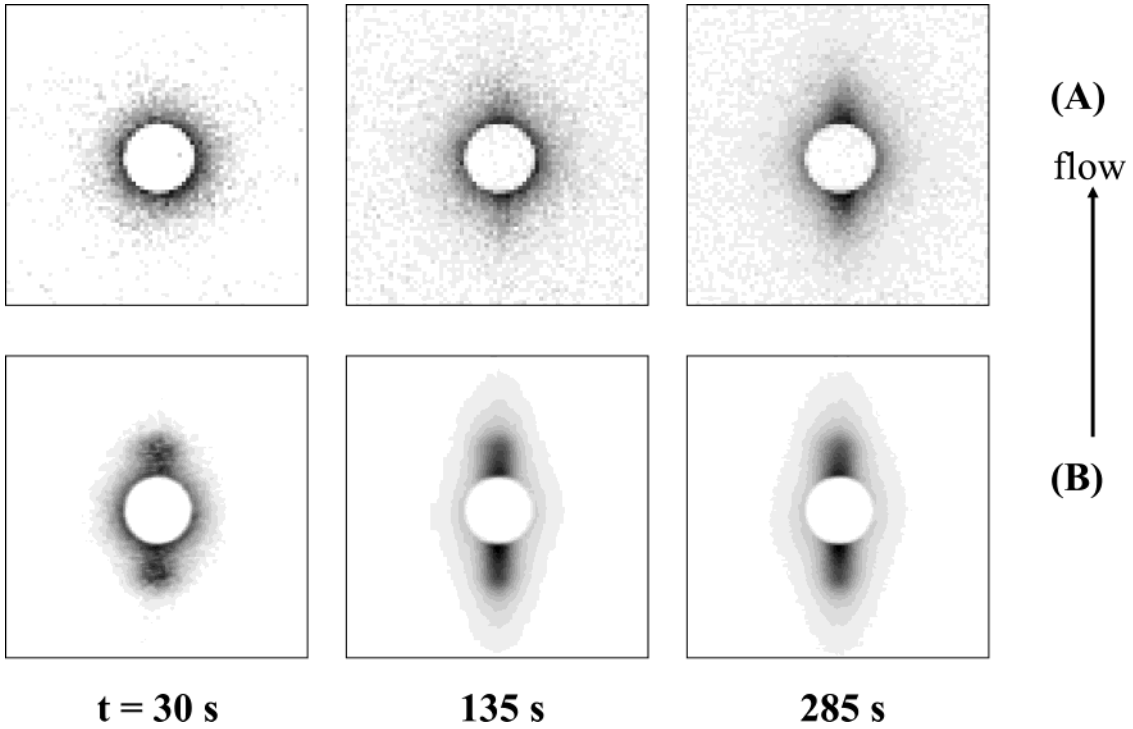

Figure 11. Selected 2D SAXS patterns of (A) MB-50K/MB-250K (95/5) and (B) MB-50K/MB-250K (90/10) after shear cessation.

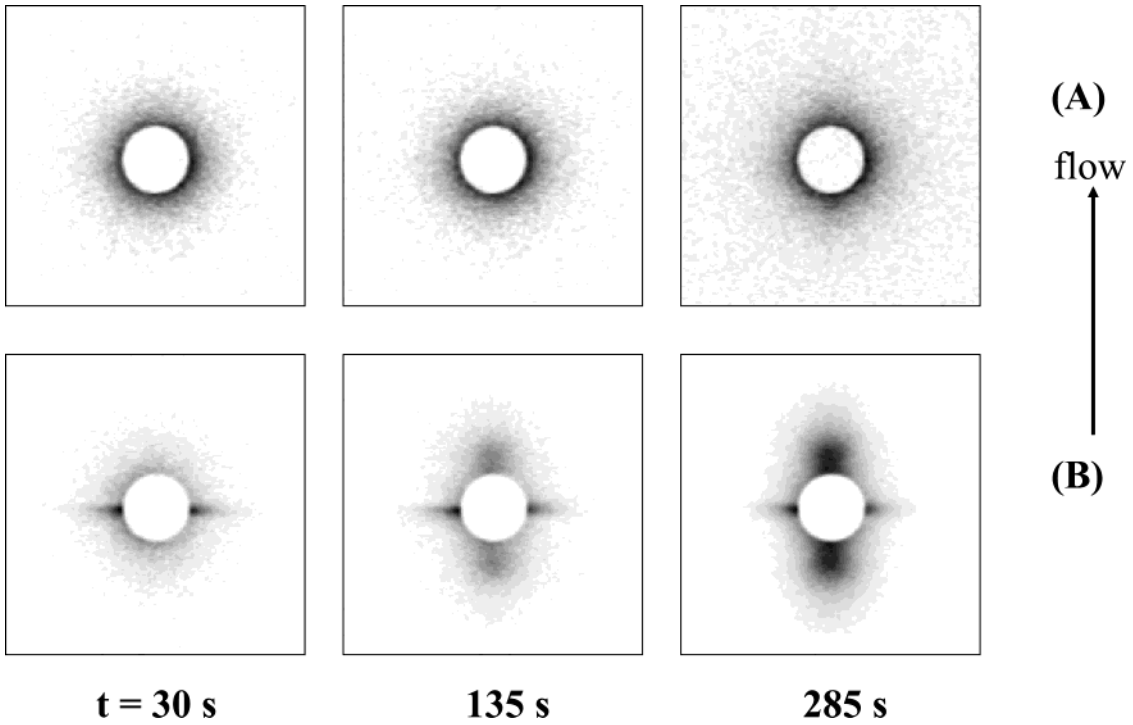

Figure 12. Selected 2D SAXS patterns of (A) MB-100K/MB-250K (95/5) and (B) MB-100K/MB-250K (90/10) after shear cessation.

and no shear as well as of the MB-100K/MB-250K (90/10) blend under no shear were carried out. Similar to the early findings of pure MB-50K, all SAXS patterns of MB-100K obtained during the experimental time frame of 45 min exhibited no scattering profile. SAXS patterns of the MB-100K/MB-250K (90/10) blend under no shear exhibited a scattering ring with no preferred orientation due to the formation of randomly distributed lamellar structures.

In Figure 12, the development of oriented superstructures was observed in both MB-100K/MB-250K (95/5) and MB-100K/MB-250K (90/10) blends after shear. The behavior of MB-100K/MB-250K (95/5) was similar to that of MB-50K/MB-250K (95/5) (Figure 11A). A pair of weak meridional scattering maxima appeared at 285 s after shear in the MB-100K/MB-250K (95/5) blend, which was later than the similar SAXS appearance of the sheared MB-50K/MB-250K (95/5) blend at 135 s. The subsequent SAXS study indicated the growth of the meridional maxima with time (not shown here), leading to the formation of well-recognized lamellar layered structures of MB-250K crystals in the melt.

SAXS patterns of the MB-100K/MB-250K (90/10) blend are remarkably different from the above observa-

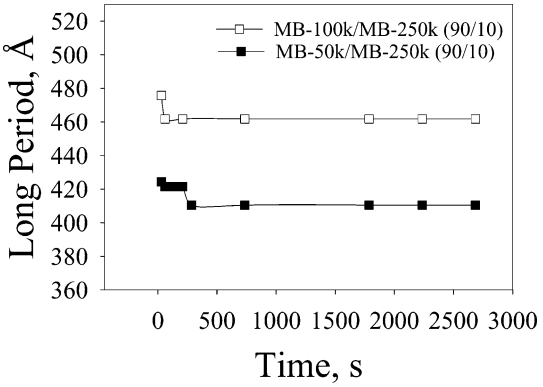

Figure 13. Variation of lamellar long period in MB-50K/MB-250K (90/10) and MB-100K/MB-250K (90/10) blends as a function of time.

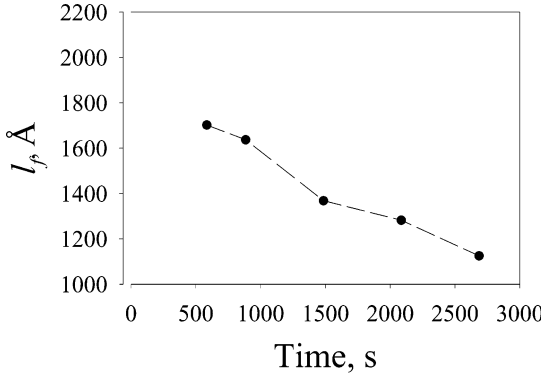

Figure 14. Length of the shish structure as a function of time in MB-100K/MB250K (90/10) blend after shear (shear rate = 60 s^{-1}, shear time = 5 s, T = 120 °C).

tions. The pattern immediately after shear (at t = 30 s) exhibited an equatorial streak with no indication of meridional maxima. The meridional maxima only emerges at a later time (t around 60 s, pattern not shown here), which could be clearly identified in the pattern at t = 135 s. Subsequently, as crystallization progressed, the equatorial and meridional scattered intensities increased with time, as seen in Figure 12B. The equatorial streak is due to the formation of a shish structure with extended-chain crystals oriented parallel to the flow direction, formed immediately after shear. The lamellar crystals, which are initiated from the shish and grow perpendicularly to the flow direction, are formed later. These results are consistent with the unique WAXD observation in the sheared MB-100K/MB-250K (90/10) blend (Figure 5B); both confirmed the formation of shish-kebab morphology at the early stages of the shear-induced crystallization.

4.6. Long Period Change between Adjacent Lamellae (Kebabs). Time evolution of the spacing between the adjacent lamellae (the long period) in MB-50K/MB-250K (90/10) and MB-100K/MB-250K (90/10) blends is shown in Figure 13. In both blends, the long period decreased slightly in the very beginning of crystallization and reached a plateau value soon afterward. For example, in the MB-50K/MB-250K (90/10) blend, the spacing decreased from 424 to 411 Å (ca. 3.5%) and remained at a constant value at t > 285 s after shear; in the MB-100K/MB-250K (90/10) blend, the spacing between adjacent lamellae decreased from 476 to 462 Å (ca. 3%) and remained constant at t > 60 s after shear. The lamellar structure in the MB-100K/MB-250K (90/10) blend was slightly larger than that in the MB-50K/MB-250K (90/10) blend. Generally, as the crystallization progresses, a slight decrease in the long period is expected as the new lamellae can form within the established superstructure. It is our opinion that the extent of the long period decrease is not substantial in these polyethylene blends after shear. Also, the difference between the plateau values of the long period for the two blends is not significant. In other words, the lamellar structures formed in these blends appear to be very similar.

4.7. Length Change of "Shish". Using the Ruland method outlined earlier, the length change of the shish structure observed in the MB-100K/MB-250K (90/10) blend was estimated. In the measured SAXS patterns at the initial stages after shear, the signal/noise ratio was too low (the current data collection time was 10 s), and the linear relationship between B_{obs} and 1/s could not be established with good statistical significance. Our attempt to increase the data collection time to improve the signal/noise ratio failed to "catch" the initial separation between the shish and kebab developments. Consequently, only the shish structure having the kebabs formed at the later stage was analyzed. The change of the shish length as a function of time is shown in Figure 14. The shish length was around 1700 Å at 585 s after shear and then decreased to around 1120 Å at the end of the experimental time (t = 2585 s). The misorientation width (eq 6) of the shish increased slightly and was not shown here. These results are quite unexpected since they indicate that the shish length is "shrinking" with the increase in the kebab formation, and the length almost decreased linearly with time. Our interpretation of this unusual behavior is presented in the Discussion section. Although the situation at the early stages could not be evaluated, we extrapolated the values of the shish length at shorter times by assuming a linear relationship between shish length and time. The estimated length of shish immediately after shear was about 1860 Å (Figure 14). It is clear that a higher X-ray beam intensity in rheo-SAXS experiments from an undulator synchrotron source would allow the direct estimate of the shish length immediately after shear.

5. Discussion

5.1. Crystallization Kinetics in Blends under Shear. The total crystallinity change and the crystallization half-time of both series of blends, MB-50K/MB-250K (100/0, 97/3, 95/5, 90/10) and MB-100K/MB-250K (100/0, 97/3, 95/5, 90/10) (Figures 6 and 7), indicate that the crystallization kinetics of the high molecular weight component (MB-250K) is a function of both concentration and viscosity of the low molecular weight matrix (short chains). We verified that the chosen two low molecular weight matrices (different in molecular weight) could not crystallize by themselves even under a relatively intense shear flow (shear rate = 60 s^{-1}, shear time = 5 s) at 120 °C in the experimental time frame (45 min). There are several reasons for this behavior. (1) The experimental temperature was 120 °C, which was slightly above the end position of the endothermic melting peak for either MB-50K or MB-100K based on the DSC data. It is conceivable that the mobility of the chains is quite high at this temperature; thus, all stretched chains can relax back to the initial "random coil" state after deformation, hindering the formation of stable nuclei. (2) Both low molecular weight components are ethylene copolymer containing 2 mol % of

hexene, which cannot be incorporated in the ethylene crystalline structure. The large copolymer composition of the matrix thus discourages the likelihood of being cocrystallized with the MB-250K component at the chosen experimental conditions.

It is interesting to note that, in general, the MB-50K/MB-250K blend exhibits a faster overall crystallization rate than the MB-100K/MB-250K blend at the same concentration levels (3, 5, and 10 wt %), as seen in Figures 7 and 8. This indicates that the molecular weight (thus the viscosity) of the matrix plays an important role in influencing the shear-induced crystallization of the high molecular weight component in the blend. This behavior should be considered by the following situations. For linear polymers, the viscosity is proportional to the molecular weight (M) with the scaling of $M^{3.4}$. Thus, MB-100K is more viscous than MB-50K, where the relaxation time spectrum of each matrix may be described by a monodisperse relaxation function.[46] (This also holds true for the high molecular weight component MB-250K.) In the bimodal polymer blend, it is known that the relaxation time spectrum of each component is governed not by its original relaxation spectrum but by the double reptation mixing rule involving relaxation spectra from both blending components, as proposed by des Cloizeaux[56] and proven by many others.[57−59] In other words, under the chosen shear conditions (i.e., constant rate and strain shearing), the resulting relaxation spectra of the high molecular weight component MB-250K in the two blends are quite different. The relaxation time spectrum of MB-250K in the MB-100K matrix should have greater values than that in the MB-50K matrix. This would have two implications. (1) The higher relaxation times of MB-250K in MB-100K may lead to a higher orientation distribution of MB-250K chains after shear, thus resulting in a higher degree of shear-induced nucleation density in the MB-100K/MB-250K blends. (2) On the other hand, the lower relaxation times of MB-250K in MB-50K should facilitate the diffusion rate of MB-250K in the matrix, which would increase the crystallization growth rate. The latter seems to be a more dominant factor on influencing the bulk kinetics properties for the chosen blends under shear.

Since the bulk crystallinity can be deconvoluted into oriented and unoriented fractions, we have also compared the developments of these two fractions in different blends. Figures 8 and 9 indicate that in the beginning of crystallization unoriented crystals develop at a faster rate in MB-50K/MB-250K (90/10) than that in MB-100K/MB-250K (90/10). At the final stage of crystallization, a slightly higher fraction of unoriented crystals is formed in MB-50K/MB-250K (90/10). These two observations are consistent with the notion that the increase in the crystal growth rate of MB-250K (due to the decrease in its viscosity) is primarily responsible for the increase in the bulk crystallization rate as well as in unoriented crystallinity. But as the relaxation time spectrum of MB-250K in the MB-100K matrix is longer than that in the MB-50K matrix, we also expect a higher density of oriented nuclei formed in the MB-100K/MB-250K blend. This was indeed observed in Figure 9, where the oriented fraction of the crystalline phase (F) in MB-100K/MB-250K is always higher than that in MB-50K/MB-250K. In Figure 9, both evolution curves of F vs crystallization time exhibit a minimum value. The initial decrease is probably due to the rapid development of unoriented crystals (through the induction of unoriented nuclei) at the initial stage of crystallization. The later "upturn" probably indicates that the growth rate from the oriented nuclei may be slightly faster than the growth rate from the unoriented nuclei. We believe that both growths (for oriented and unoriented lamellae) are initiated from the coiled chains (unstretched chains) of MB-250K, which will be discussed further later.

Comparing the crystallization rate under shear and quiescent conditions, we find that the rate under shear only increases slightly (Figure 12). This increase is mainly due to the increase in nucleation density through the deformation of the MB-250K component. This is consistent with the notion that the nucleation is initiated from the stretched segments of the MB-250K chains. The crystal growth rate of the MB-250K chains (dictated by the viscosity) appears to remain about constant between the shear and quiescent conditions, which is expected. In fact, it is interesting to see that once the unoriented crystals start to develop, the growth rate of MB-250K in the quiescent state of the MB-100K/MB-250K blend becomes even higher than that obtained in the sheared state at 120 °C (Figure 10).

5.2. Formation of Crystallization Precursor Structures. The pathway of crystallization in polymer melt under flow has been a subject of intense interest for decades. In our recent study,[9] we have outlined the possible mechanism for the formation of precursor structures under flow, prior to the event of full-scale crystallization. In this study, we not only confirmed this hypothesis but also obtained some new insights into the mechanism in polyethylene by using the model blends.

5.2.1. Effect of Long Chains on Formation of Shish. Blending a small amount of higher molecular weight polyethylene (longer chain species) into the lower molecular weight polyethylene matrix undoubtedly affects many aspects of crystallization behavior as well as the morphology of the blend under both quiescent and flow conditions. Although we expect that the relaxation time spectra of the high molecular weight component (MB-250K) are quite different in the matrices of different low molecular weights (e.g., lower value in the MB-50K matrix and higher value in the MB-100K matrix), it is still surprising to detect the sharp distinction in the structure and morphology observed between the MB-100K/MB-250K (90/10) blend and the rest of the samples under shear. In the MB-100K/MB-250K (90/10) blend under shear, there is no question that the initial development of the equatorial "streak" in SAXS and the simultaneous appearance of two equatorial (110) reflections in WAXD (Figure 15) clearly indicate the formation of a "shish" structure with a length on the order of 1000 Å (Figure 14) and a diameter on the order of 100 Å (based on the crystallite size analysis of the equatorial (110) peak using the Scherrer equation[60]) similarly found by the scientists using the microscopic techniques.[26,38,61] However, for the rest of the blends, such a "shish" structure is not seen, which is most interesting.

The immediate formation of a relatively large shish structure in the MB-100K/MB-250K (90/10) blend upon the cessation of shear indicates that the crystallization process starts in highly oriented MB-250K chains. The crystallization process in this case will be very fast, dictated only by the rapid alignment of the chains due to imposed flow condition. If the oriented MB-250K

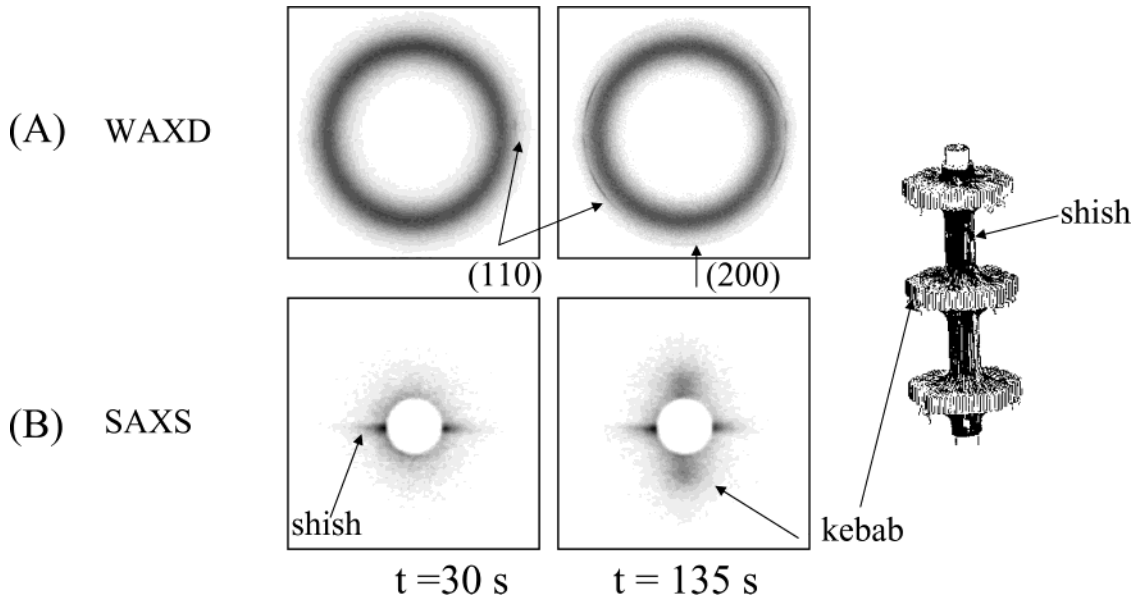

Figure 15. Selected 2D (A) WAXD and (B) SAXS patterns to illustrate development of "shish-kebab" morphology[5] in PE blends.

chains are randomly dispersed in the lower molecular weight matrix (MB-50K or MB-100K), the formation of shish would require the lateral translation of oriented chains, which is easier and more likely to be observed in the case of blend with high concentration (10%) of MB-250K than the low-concentration blends. Note that despite the lack of the shish formation, the existence of oriented chains or oriented segments of chains can effectively nucleate the kebab structure, which has recently been demonstrated by molecular modeling work[44,45] and will be discussed further in the later sections. We term these oriented chains or segments of chains as fibrillar extended-chain precursor structures of oriented primary nuclei.

The other dominant factor responsible for the formation of shish is the local stress experienced by polymer molecules, especially those involved in its formation (MB-250K chains), which is quite different in these blends. This is because the chosen experimental conditions involved constant strain and constant rate, and thus the stress distributions within each blend should vary quite substantially. As the MB-100K/MB-250K (90/10) blend has the highest value of relaxation time spectrum, the local stress imposed on the MB250K chain is probably the highest when compared to those in the rest of the blends.

5.2.2. Formation of Oriented Twisted Lamellae. Upon the cessation of shear, all chosen blends exhibited oriented lamellae (or kebabs), regardless of the appearance of "shish". When shish was detected (in the MB-100K/MB-250K (90/10) blend), kebabs were always formed afterward. The mechanism for the shish-kebab formation probably refers to the recent modeling work of Muthukumar et al.,[44] which suggests that shish resulted from the extended-chain crystallization of stretched (or oriented) chains and kebabs resulted from the folded-chain crystallization of coiled chains, which are subsequently attached to shish. It is interesting to note that in most blends the detection of shish by SAXS and WAXD was not seen. We believe that the presence of "shish" in these cases only consists of a small bundle of aligned chains (or chain segments), which are not detectable by X-ray scattering/diffraction or microscopy. However, the general mechanism for the shish-kebab formation probably should still hold true here. Thus, the flow-induced "shish" structure in these blends, though invisible, probably resembles the fibrillar extended-chain structure that may be mesomorphic or partly crystalline, instead of the fibrillar-like extended-chain crystal.[61]

On the basis of our WAXD data, we conclude that all shear-induced lamellae in PE eventually develop into a twisted structure, which is verified by the unique appearance of the (200) reflection. For example, in Figures 4 and 5, a pair of (200) reflections is seen in the meridional direction at the intermediate stages of crystallization. If the lamellar structure is flat (this probably occurs at the initial stages of the lamellar formation after flow), the *c*-axis of the crystals should be aligned parallel to the flow direction and the *b*-axis should be perpendicular to the flow direction. This would result in the appearance of two (200) reflections on the equator, which was not seen in this study. If twisted lamellae are developed during growth, as previously reported by Keller and Schultz in flow-induced crystallization of PE,[5,55] the crystal *a*- and *c*-axes would rotate around the *b*-axis, resulting in the changes of the (200) reflection from equatorial alignment to meridional alignment. The twisted lamellar structure is also consistent with the appearance of four (110) reflection peaks at the off-axis positions.

5.2.3. Evolution of Shish-Kebab Morphology after Shear. In Figure 13, it is noticed that the long period of the adjacent MB-250K lamellae in the MB-100K/MB-250K (90/10) blend is higher than that in the MB-50K/MB-250K (90/10) blend, where both values show immediate decreases with time during crystallization. The higher long period suggests a lower nucleation density in MB-100K/MB-250K (90/10). As each kebab is developed through the adsorption of coil chains on the shish, a stress distribution must be generated in the vicinity of the kebab (folded-chain lamella). We speculate that the stress distribution surrounding a formed kebab on the shish within the crystallizing domain of a higher degree of orientation (the MB-100K/MB-250K (90/10) blend) must be higher than that within the domain of a lower degree of orientation (e.g., the MB-50K/MB-250K (90/10) blend),

preventing the generation of a higher kebab density (or a lower long period value). The rapid long period decrease (3−4%) at the initial stages of crystallization is probably due to the space-filling nature (such as lamellar insertion on the shish) of crystallization in MB-250K chains, which has been seen in crystallization in many polymers under isothermal conditions.[62]

The changes of the "visible" shish-kebab structure in the MB-100K/MB-250K (90/10) blend were analyzed to monitor the stability of shish-kebab after the cessation of flow and during the process of crystallization. Our results indicate that the shish length decreases with time in a nearly linear fashion (Figure 14), while the corresponding intensity increases continuously. Peterman et al.[59] proposed that the shish formation involves an autocatalytic process in the nuclei growth along the flow direction, where the growth process is maintained and/or enforced by a self-induced orientation of the molecules in front of the growing tip. This is opposite to our finding here. Perhaps the process proposed by Peterman et al. holds true only in the initial stages of shish formation under flow, whereas our results were obtained during the later stages of shish development upon the cessation of flow. The decrease in the "shish length" suggests that the development of kebabs may have relaxed the total orientation of the shish (fibrillar-like extended-chain crystals) by introducing spatial dependent local stress distributions, thus "shortening" the overall projection length of the shish-kebab entity (the true length of the shish is preserved). The increase of the shish scattered intensity is probably due to the improved density contrast (between crystalline precursor structure and amorphous surroundings) and the increasing volume fraction of the shish-kebab entity during lamellar growth.

6. Conclusions

Using time-resolved SAXS and WAXD techniques and model binary PE blends (MB-50K/MB-250K (100/0, 97/3, 95/5, 90/10) and MB-100K/MB-250K (100/0, 97/3, 95/5, 90/10)), we have obtained several new insights into the development of crystallization precursor structures by shear (rate = 60 s^{-1}, duration = 5 s, T = 120 °C) prior to the occurrence of full-scale crystallization. The unique feature of these blends is that the low molecular weight matrix (MB-50K or MB-100K) does not crystallize under the experimental conditions where only the high molecular weight additive can form the scaffold of precursor structure. These new insights can be summarized as follows.

1. Both chemical composition and applied shear flow can significantly affect the crystallization kinetics of the crystallizing high molecular weight component (MB-250K), but in a very different fashion since the viscosity (thus the relaxation time spectrum) of the high molecular weight component is changed cooperatively with the viscosity of the matrix. When the viscosity of the matrix is low, the viscosity of the crystallizing high molecular weight component also becomes lower, leading to faster crystal growth under both quiescent and flow conditions. In contrast, when the viscosity of the matrix is high, the viscosity of the crystallizing high molecular weight component becomes higher, which favors the development of higher nucleation density induced under flow (e.g., the composition of 10 wt % of MB-250K exhibited the fastest crystallization rate in the MB-100K/MB-250K blends).

2. In the MB-100K/MB-250K (90/10) blend, both rheo-SAXS and rheo-WAXD patterns showed the formation of distinct "shish-kebab" morphology having a "length" over 1000 Å, while the rest of the blends only exhibited oriented lamellar (kebab) morphology without the presence of shish. The observed "shish" structure can be attributed to the extended-chain crystallization of stretched PE chain segments. In addition, all formed kebabs exhibited a twisted lamellar structure, typically seen in PE crystallites formed from chains of no orientation. We speculate that the observed shish is related to the high values of relaxation time spectrum in MB-250K, where the corresponding high values of local stress promote the rapid alignment of chains. In other blends, as the stretched chains do not aggregate rapidly, no detectable shish was observed. However, the pathway of the "shish-kebab" or "oriented kebab" formation clearly follows the concept of "coil−stretch" transition first proposed by Keller et al.[5] and later demonstrated by Muthukumar et al.[44] using simulation tools.

3. The decrease in the shish length with time in the MB-50K/MB-250K (90/10) blend is probably due to the decrease of orientation in flow-induced extended-chain crystals (shish) due to the development of lamellae (kebabs) through folded-chain crystallization. In other words, the projection length of the "shish-kebab" structure becomes shortened with the relaxation of stress distribution or the overall crystal orientation.

Acknowledgment. We acknowledge the assistance of Drs. Fengji Yeh, Lizhi Liu, Dufei Fang, Shaofeng Ran, and Carlos A. Avila-Orta for synchrotron SAXS and WAXD experimental setup. The National Science Foundation (DMR-0098104 and DMR-0405432) and the ExxonMobil Company provided the financial support of this work.

References and Notes

(1) Flory, P. J. *J. Chem. Phys.* **1947**, *15*, 397.
(2) Ward, I. M. *Structure and Properties of Oriented Polymers*; Wiley: New York, 1975.
(3) Ziabicki, A. *Fundamentals of Fiber Formation*; Wiley: New York, 1976.
(4) Ziabicki, A., Kawai, H., Eds.; *High-Speed Fiber Spinning*; Interscience: New York, 1985.
(5) Keller, A.; Kolnaar, H. W. *Mater. Sci. Technol.* **1997**, *18*, 189.
(6) Eder, G.; Janeschitz-Kriegl, H. *Mater. Sci. Technol.* **1997**, *18*, 268.
(7) Wilkinson, A. N.; Ryan, A. J. *Polymer Processing and Structure Development;* Kluwer: Dordrecht, 1998.
(8) Lee, O.; Kamal, M. R. *Polym. Eng. Sci.* **1999**, *39*, 236.
(9) Somani, R. H.; Yang, L.; Hsiao, B. S.; Agarwal, P. K.; Fruitwala, H. A.; Tsou, A. H. *Macromolecules* **2002**, *35*, 9096.
(10) Jerschow, P.; Janeschitz-Kriegl, H. *Int. Polym. Process.* **1997**, *12*, 72.
(11) Duplay, C.; Price, F.; Stein, R. *J. Polym. Sci., Polym. Symp.* **1978**, *63*, 77.
(12) Lagasse, R. R.; Maxwell, B. *Polym. Eng. Sci.* **1976**, *16*, 189.
(13) Vleeshouwers, S.; Meijer, H. *Rheol. Acta* **1996**, *35*, 391.
(14) Keller, A.; Odell, J. A. *Colloid Polym. Sci.* **1985**, *263*, 181.
(15) Seki, M.; Thurman, D. W.; Oberhauser, J. P.; Kornfield, J. A. *Macromolecules* **2002**, *35*, 2583.
(16) Somani, R. H.; Hsiao, B. S.; Nogales, A.; Srinivas, S.; Tsou, A. H.; Sics, I.; Balta-Calleja, F. J.; Ezquerra, T. A. *Macromolecules* **2000**, *33*, 9385.
(17) Nogales, A.; Hsiao, B. S.; Somani, R. H.; Srinivas, S.; Tsou, A. H.; Balta-Calleja, F. J.; Ezquerra, T. A. *Polymer* **2001**, *42*, 5247.
(18) Somani, R. H.; Hsiao, B. S.; Nogales, A.; Fruitwala, H.; Srinivas, S.; Tsou, A. H. *Macromolecules* **2001**, *34*, 5902.
(19) Somani, R. H.; Yang, L.; Hsiao, B. S. *Physica A* **2002**, *304*, 145.
(20) Somani, R. H.; Yang, L.; Sics, I.; Hsiao, B. S.; Pogodina, N. V.; Winter, H. H.; Agarwal, P.; Fruitwala, H.; Tsou, A. *Macromol. Symp.* **2002**, *185*, 105.

(21) Pope, D. P.; Keller, A. *Colloid Polym. Sci.* **1978**, *256*, 751.
(22) Miles, M. J.; Keller, A. *Polymer* **1980**, *21*, 1295.
(23) Mackley, M. R.; Frank, F. C.; Keller, A. *J. Mater. Sci.* **1975**, *10*, 1501.
(24) Hill, M. J.; Keller, A. *J. Macromol. Sci., Phys.* **1969**, *B3*, 153.
(25) Hill, M. J.; Keller, A. *J. Macromol. Sci., Phys.* **1971**, *B5*, 591.
(26) Pennings, A. J.; van der Mark, J. M. A. A.; Kiel, A. M. *Kolloid Z. Z. Polym.* **1970**, *237*, 336.
(27) Wereta, A.; Gogos, C. *Polym. Eng. Sci.* **1971**, *11*, 19.
(28) Ulrich, R. D.; Price, F. P. *J. Appl. Polym. Sci.* **1976**, *20*, 1077.
(29) Eder, G.; Janeschitz-Kriegl, H.; Liedauer, S. *Prog. Polym. Sci.* **1990**, *15*, 629.
(30) Bayer, R. K.; Eliah, A. E.; Seferis, J. C. *Polym. Eng. Rev.* **1984**, *4*, 201.
(31) Liedauer, S.; Eder, G.; Janeschitz-Kriegl, H. *Int. Polym. Process.* **1995**, *10*, 243.
(32) Jerschow, P.; Janeschitz-Kriegl, H. *Int. Polym. Process.* **1997**, *12*, 72.
(33) Kumaraswamy, G.; Issaian, A. M.; Kornfield, J. A. *Macromolecules* **1999**, *32*, 7537.
(34) Kumaraswamy, G.; Verma, R. K.; Issaian, A. M.; Wang, P.; Kornfield, J. A.; Yeh, F.; Hsiao, B. S.; Olley, R. H. *Polymer* **2000**, *41*, 8931.
(35) Kumaraswamy, G.; Kornfield, J. A.; Yeh, F.; Hsiao, B. S. *Macromolecules* **2002**, *35*, 1762.
(36) Kornfield, J. A.; Kumaraswamy, G.; Issaian, A. M. *Ind. Eng. Chem. Res.* **2002**, *41*, 6383.
(37) Agarwal, P. K.; Somani, R. H.; Weng, W.; Mehta, A.; Yang, L.; Ran, S.; Liu, L.; Hsiao, B. S. *Macromolecules* **2003**, *36*, 5226.
(38) Hobbs, J. K.; Miles, M. J. *Macromolecules* **2001**, *34*, 353.
(39) Hobbs, J. K.; Humphris, A. D. L.; Miles, M. J. *Macromolecules* **2001**, *34*, 5508.
(40) Welch, P.; Muthukumar, M. *Phys. Rev. Lett.* **2001**, *87*, No. 21.
(41) Liu, C.; Muthukumar, M. *J. Chem. Phys.* **1998**, *109*, 2536.
(42) Welch, P.; Muthukumar, M. *Polymer* **2000**, *41*, 8833.
(43) Muthukumar, M. *Eur. Phys. J. E: Soft Matter* **2000**, *3*, 199.
(44) Dukovski, I.; Muthukumar, M. *J. Chem. Phys.* **2003**, *118*, 6648.
(45) Hu, W.; Frenkel, D.; Mathot, V. B. F. *Macromolecules* **2002**, *35*, 7172.
(46) Ferry, J. D. *Viscoelastic Properties of Polymers*, 3rd ed.; Wiley: New York, 1980.
(47) Reichart, G. C.; Graessley, W. W.; Register, R. A.; Lohse, D. J.; *Macromolecules* **1998**, *31*, 7886.
(48) Han, S. J.; Lohse, D. J.; Condo, P. D.; Sperling, L. H. *J. Polym. Sci., Phys.* **1999**, *37*, 2835.
(49) Takahashi, Y.; Isono, Y.; Noda, I.; Nagasawa, M. *Macromolecules* **1985**, *18*, 1002.
(50) Fetters, L. J.; Lohse, D. J.; García-Franco, C. A.; Brant, P.; Richter, D. *Macromolecules* **2002**, *35*, 10096.
(51) Ran, S.; Zong, X.; Fang, D.; Hsiao, B. S.; Chu, C. *J. Appl. Crystallogr.* **2000**, *33*, 1031.
(52) Ruland, W. *Colloid Polym. Sci.* **1978**, *256*, 932.
(53) Ruland, W. *J. Polym. Sci., Part C* **1969**, *28*, 143.
(54) Ran, S.; Fang, D.; Zong, X.; Hsiao, B. S.; Chu, B.; Cunniff, P. M. *Polymer* **2001**, *42*, 1601.
(55) Nadkarni, V. M.; Schultz, J. M. *J. Polym. Sci., Polym. Phys. Ed.* **1977**, *15*, 2151.
(56) des Cloizeaux, J. J. *Europhys. Lett.* **1988**, *5*, 437.
(57) Wasserman, S. H.; Graessley, W. W. *J. Rheol.* **1992**, *36*, 543.
(58) Mead, D. W. *J. Rheol.* **1994**, *38*, 1797.
(59) McGrory, W. J.; Tuminello, W. H. *J. Rheol.* **1990**, *34*, 867.
(60) Alexander, L. E. *X-Ray Diffraction Methods in Polymer Science*; Wiley: New York, 1969.
(61) Lieberwirth, I.; Loos, J.; Petermann, J.; Keller, A. *J. Polym. Sci., Part B: Polym. Phys.* **2000**, *38*, 2583.
(62) Verma, R. K.; Hsiao, B. S. *Trends Polym. Sci.* **1996**, *4*, 312.

MA049925F